

**INTER-AMERICAN TROPICAL TUNA COMMISSION**

**SCIENTIFIC ADVISORY COMMITTEE**

**SIXTH MEETING**

**La Jolla, California (USA)**

**11-14 May 2015**

**DOCUMENT SAC-06 INF-C**

**OCEANOGRAPHIC CONDITIONS IN THE EPO AND THEIR EFFECTS  
ON TUNA FISHERIES**

**Michael G. Hinton**

1. Introduction.....	1
2. Oceanography in the EPO.....	1
3. Historical trends in oceanographic conditions.....	10
4. Current and predicted oceanographic conditions .....	11
5. Oceanographic impacts on tuna stocks, fisheries, and management.....	12
6. Current research.....	15
7. Summary.....	20
8. Literature cited.....	20

**1. INTRODUCTION**

This report describes the oceanography in the eastern Pacific Ocean (EPO), and reviews historical trends in ocean climate and regimes and current conditions. The relationships between variations in ocean conditions and impacts on the tuna stocks, and the fisheries that harvest them (IATTC 2014), are discussed. Ongoing research expected to provide tools to enhance management of the fisheries resources of the EPO is presented.

**2. OCEANOGRAPHY IN THE EPO**

The principal surface currents comprising the equatorial current system are shown in [Figure 1](#). Three of these, the North Equatorial Current (NEC), the South Equatorial Current (SEC), and the North Equatorial Countercurrent (NECC), are surface currents. The fourth is the subsurface Equatorial Undercurrent (EUC), whose position is constrained to the equator (Cromwell 1958). The large-scale wind-driven surface current circulation is maintained by energy transfer to the ocean surface by the north- and south-easterly trade winds that circle the globe between about 30°S and 30°N and that converge at the Inter-Tropical Convergence Zone (ITCZ), and by the Westerlies, which occur between latitudes 35° and 50° in both hemispheres ([Figure 2](#)).

The Coriolis force, which is induced by the rotation of the earth acting on wind and ocean currents, causes westward-flowing currents to veer to the right in the northern hemisphere, and to the left in the southern hemisphere.

The opposite applies to eastward-flowing currents. As the NEC and SEC reach the western rim of the Pacific Ocean basin, they are redirected (consistent with the Coriolis force) towards the poles, creating the western-boundary Kuroshio and the Eastern Australian currents. The poleward-flowing Kuroshio Current eventually flows into the North Pacific Current, which, on striking the North American continent, turns south and gives rise to the California Current, which then merges into the NECC at about 25°N, completing the current system encircling the North Pacific Gyre. The Eastern Australian Current flows southward until it merges into the eastward-flowing Antarctic Circumpolar Current (ACC), which, on reaching the South American continent, divides, and a portion of it flows north as the Humboldt Current, thereby completing the encirclement of the South Pacific Gyre.

The effect of wind on surface waters creates a phenomenon known as Ekman Transport, which causes water from the currents encircling the gyres to flow into their centers, raising the height of the sea surface. This causes downwelling as the water in the gyres is forced downwards.

The wind-driven currents are not centered on the equator, due to the southeasterly orientation of the coastline of the Americas and of the location of gaps in the mountain ranges of Mexico and Central America (Amador *et al.* 2006), which cause a shift of the trade winds to the north. These currents vary in velocity with the seasonal strengthening of the trade winds during the northern-hemisphere (boreal) winter. The North Equatorial Current (NEC), located at about 10-15°N, flows westward at about 20 cm/sec (0.4 knots); the South Equatorial Current (SEC), which straddles the equator between about 7°N and 15°S, flows westward at about 100 cm/sec (2 knots); and the North Equatorial Countercurrent (NECC), located between the NEC and SEC at about 3°N-10°N,

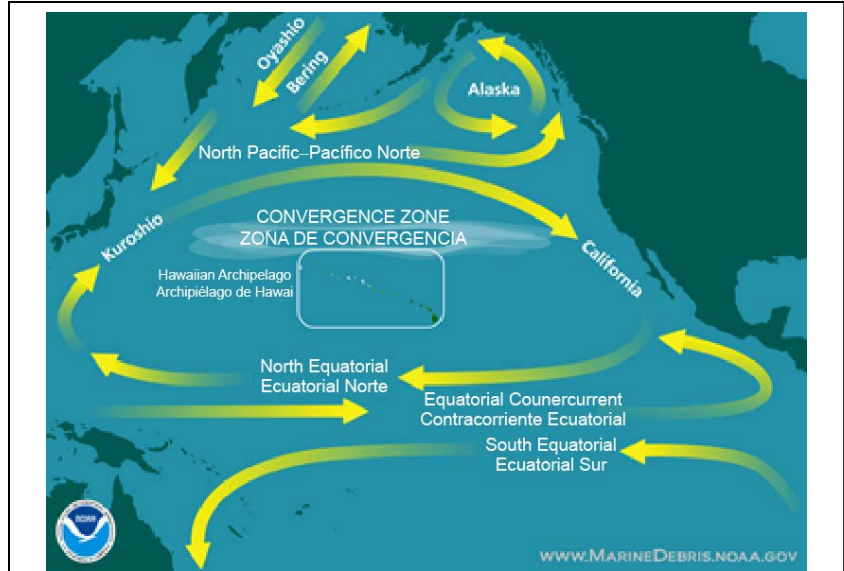


**FIGURE 1.** Surface currents of the northern and equatorial Pacific Ocean. (<http://marinedebris.noaa.gov/>)

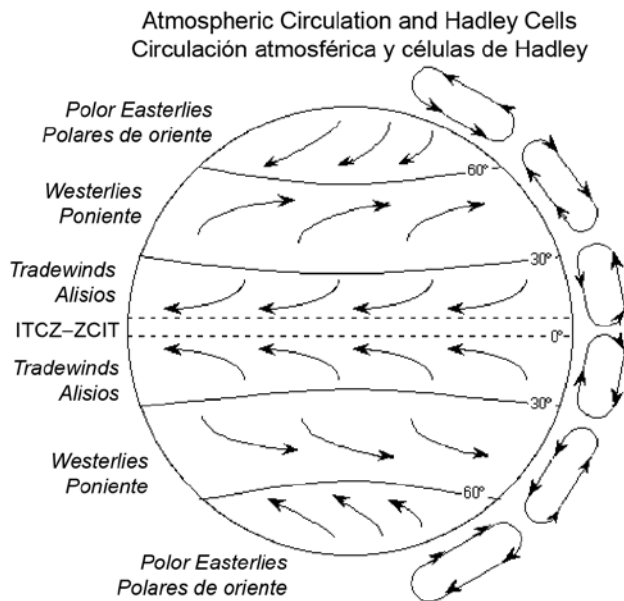


**FIGURE 2.** General surface wind and meridional Hadley Circulation. Note the north and south Hadley cells have upward flow at the ITCZ and downward flow at 30° latitude.

([http://rjwsciencestm.com/Weather/Weather\\_FourWinds.html](http://rjwsciencestm.com/Weather/Weather_FourWinds.html))

and the North Equatorial Countercurrent (NECC), located between the NEC and SEC at about 3°N-10°N,

flows eastward at about 50 cm/sec (1 knot). At the interface of the NECC and SEC, current shear, which results from the friction between two currents that are in contact but are not moving in the same direction or at the same speed, causes cyclonic eddies that are entrained in the SEC and move southwest with the current. The equatorial current system varies in intensity in response to seasonal changes in wind forcing and because the Coriolis force diminishes with current velocity and latitude, dropping to zero at the equator. These changes in dynamics lead to changes in all key oceanographic parameters in the EPO, among them upwelling, ring and eddy formation and movement, primary production, thermocline topography, and sea surface temperature (SST).

Representative distributions of monthly average SSTs for regions with SSTs in the 24°-30°C range are shown in [Figure 3](#). This temperature range was chosen both because spawning of tunas and about 90 percent of the catch of yellowfin tuna (*Thunnus albacares*; YFT) occur at these SSTs. The expansion and contraction of these areas lags the atmospheric seasons due to the rate of transfer of solar energy to the ocean surface and its subsequent redistribution by physical forcing. The distribution of SSTs undergoes significant shifts at frequencies greater than the seasonal cycle, with the largest changes occurring during El Niño and La Niña events (see below).

The thermocline is the location in the water column at which the change in temperature with increasing depth is the greatest. Taking the 20°C isotherm to represent the depth of the thermocline, the north-south, or meridional, thermal structure in the EPO is shown in [Figure 4](#). The transect runs from 17°S to 20°N at about 155°W. Following the 20°C isotherm from the south (left), the thermocline shoals from about 250 m at 17°S to about 150 m at the equator, at the center of the EUC, then descends to about 180 m at about 4°N, below the NECC. It then begins to shoal again as it continues to pass under the NECC, and reaches its shallowest depth, about 90 m, directly below the convergence of the NECC and the NEC. Thereafter it continues to descend as it passes beneath the NEC and the northern gyre. This pattern is evident from 155°W to about 160°E, and east to about 90°W, becoming less pronounced to the west and

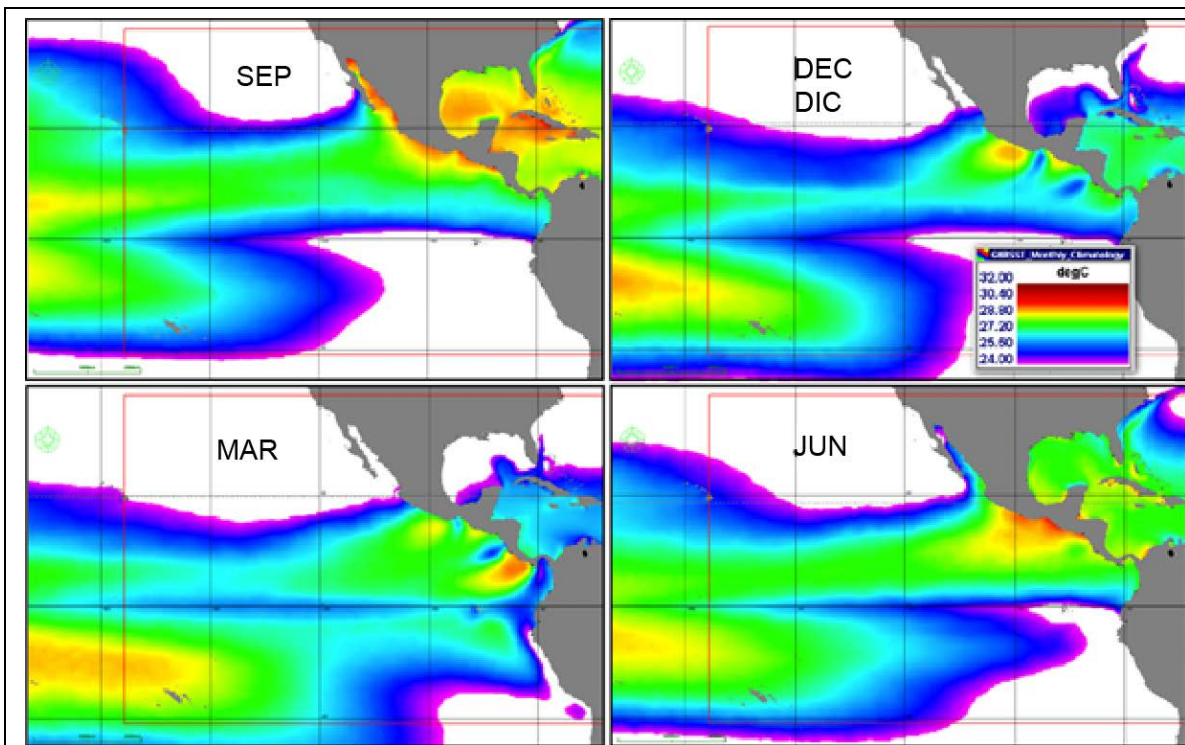


**FIGURE 3.** Distribution of the quarterly average SST between 24° and 32°C. The lower limit is the minimum temperature for spawning for tunas, and 90% of the yellowfin catch is taken from waters within this temperature range. (image: EASy/Spatial Analysis)

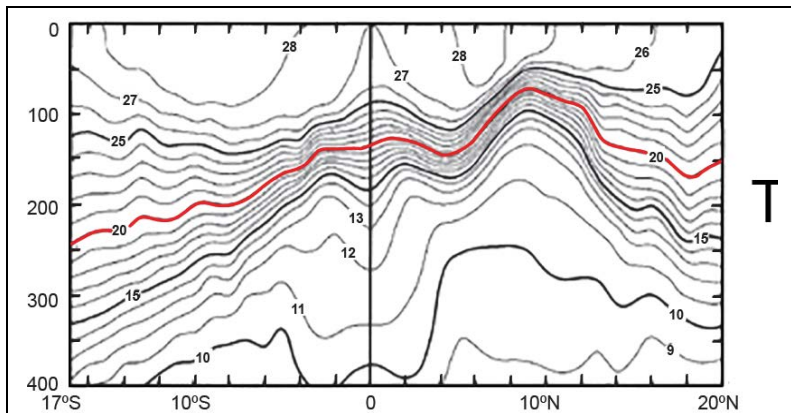


**FIGURE 4.** Meridional transect of the 20°C isotherm between 17°S and 20°N at about 155°W. The 20°C isotherm serves to represent the depth of the thermocline (Adapted from Figure 2, Wyrтки and Kilonsky 1984).

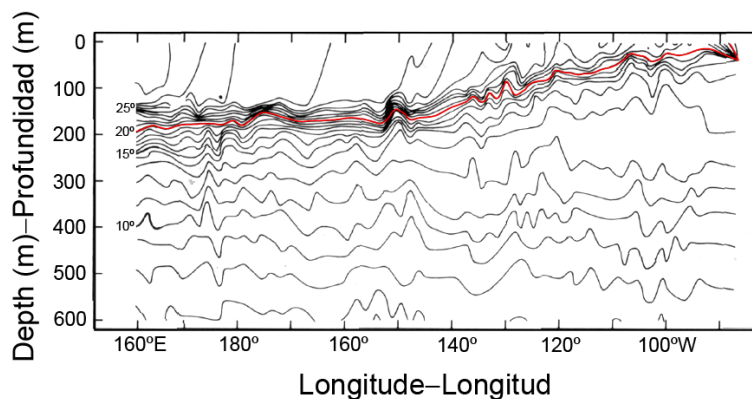


**FIGURE 5.** Zonal transect of the 20°C isotherm showing shoaling between 160°E and 90°W (Philander 1990).

more pronounced to the east. The zonal, or east-west, thermocline structure is presented in [Figure 5](#). It shows that at the equator the thermocline shoals from a depth of about 200 m at 160°E to 40 m at 90°W. The thermocline plane may be visualized as a ridge rising from the west along the equator and dropping off to the north and south thereof. During El Niño events, the thermocline ridge shoals in the west and deepens in the east, and the thermocline plane flattens out as warmer surface water spreads over the central and eastern Pacific.

The EPO is characterized by a strong, shallow oxygen minimum area beneath the thermocline that limits the vertical distributions of fish and restricts secondary production. The depth of this zone is closely linked to the depth of the thermocline, and the areas with the lowest oxygen levels coincide with the areas with the shallowest thermoclines. [Figure 6](#) shows the oxygen concentration (ml/l) at a depth of 150 m. The region of lowest oxygen concentrations in the northern EPO extends offshore from

the coast between the NEC and SEC (Pennington *et al.* 2006). Oxygen is depleted at depth in this region by decaying organic matter that sinks below the thermocline from the higher production areas above, and these oxygen-depleted waters spread across the EPO beneath the thermocline.

Productivity in the equatorial and northern EPO is controlled by the availability of nutrients in the euphotic zone, the region in the water column that receives enough light for photosynthesis. The principal regions of primary production in the EPO are in upwelling regions along the coasts and the equator and downstream of the Costa Rica Dome ([Figure 7](#)). Upwelling off the coasts is enhanced by longshore winds and the resulting offshore movement of water (Ekman Transport). Upwelling at the Dome results from a combination of shoaling of the thermocline due to wind forcing and the resulting Ekman Transport, the synchronous offshore movement of the Dome and extension of the NECC to the coast south of the Dome, and the deepening of the Dome caused by high-velocity trade winds in mid-winter (Fiedler 2002). Higher productivity near the coast and in the region west of Ecuador and northern Peru results from coastal upwelling into the Humboldt Current and its extension into the SEC from long-shore winds and Ekman Transport.

The nutricline, the depth at which the gradient of increasing nutrient concentration is greatest, coincides with the depth of the thermocline in all oceans (Pennington *et al.* 2006). Upward mixing of recycled nutrients from below the thermocline into the euphotic zone supports primary production in the nutricline. About 22% of the primary production in the Pacific Ocean comes from the EPO, which covers only about

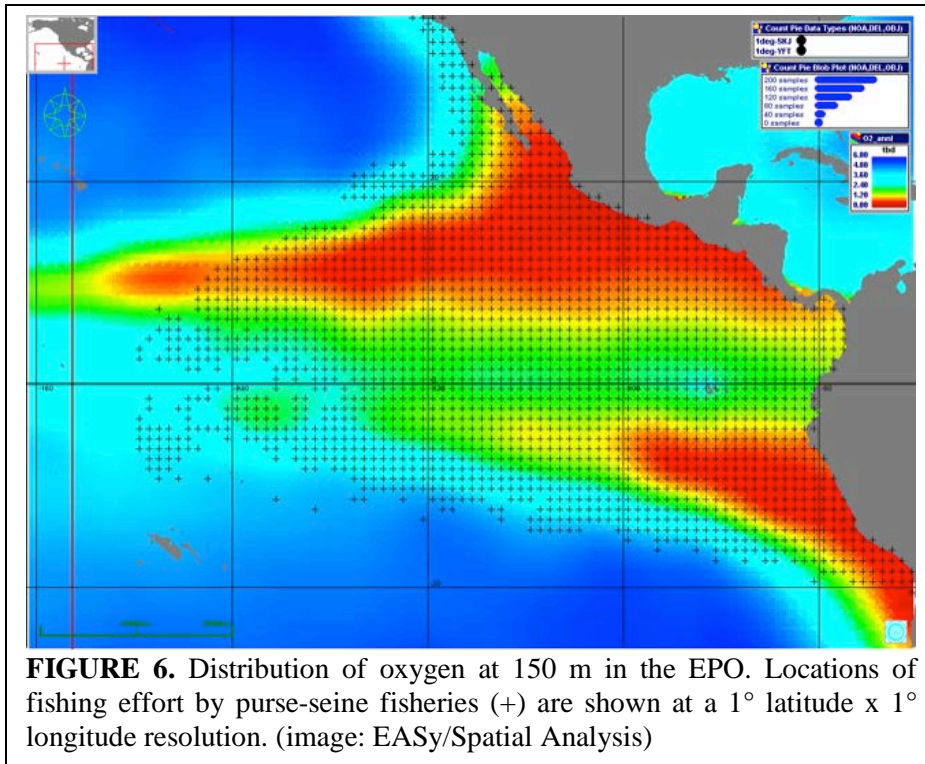


**FIGURE 6.** Distribution of oxygen at 150 m in the EPO. Locations of fishing effort by purse-seine fisheries (+) are shown at a 1° latitude x 1° longitude resolution. (image: EASy/Spatial Analysis)

18% of the Pacific Ocean. Within the EPO, the principal contributors to this production are the eastern boundary currents (21.4%), the SEC (17.5%), the coastal boundaries (16.1%), equatorial upwelling (13.6%), and the south Pacific gyre (11.4%). The remaining 20% comes from the NEC, NECC, and the thermocline ridge at 10°N (Pennington *et al.* 2006). [Figure 8.](#) shows the distribution of chlorophyll, which indicates primary production, in February 2007. The regions of

highest productivity are clearly visible. In most oceans, primary production is limited by the availability of nutrients, but in the EPO it is limited by low concentrations of iron. However, in upwelling regions along the coast, in the vicinity of the Galapagos Islands, and at the equator, iron is available, and creates the areas of relatively high production in the EPO (Pennington *et al.* 2006).

Multiple measures (see below) have served as indicators of the onset and subsequent decay of El Niño

events. The earliest indicator of an El Niño in the EPO is an increase in the southern extent of the surface countercurrent flowing southward along the coast of Ecuador. This current, known locally as El Niño, is formed in the winter months (January-March/April) by a southward-flowing extension of the NECC (Sverdrup *et al.* 1942) and a portion of the flow of the EUC (Philander 1990) that turns south as it passes the Galapagos Islands. In El Niño years, the annual intensification of the EUC during the winter months is stronger than average.

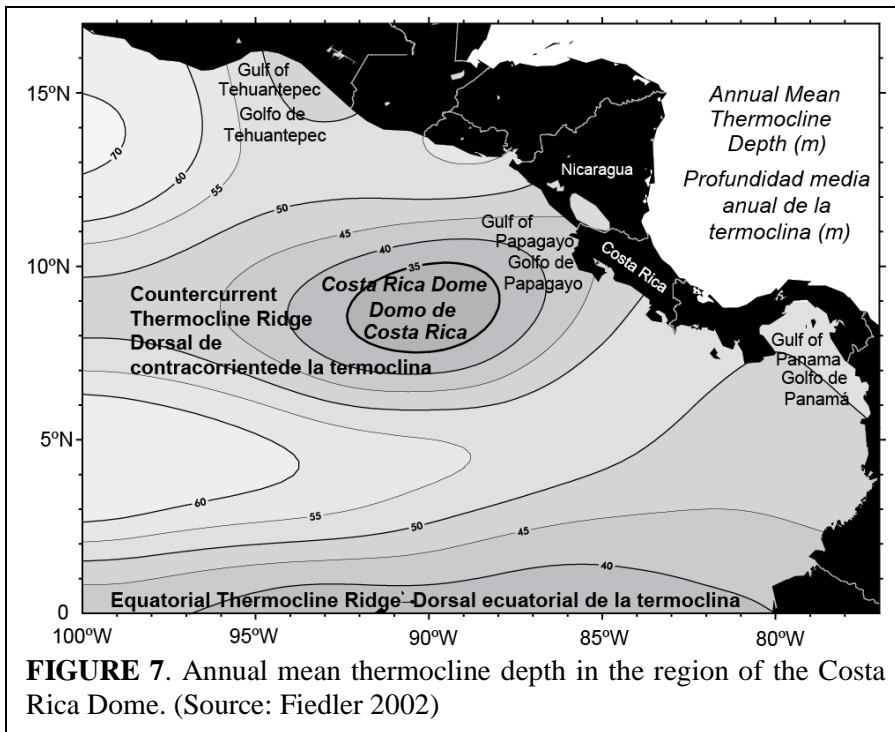


**FIGURE 7.** Annual mean thermocline depth in the region of the Costa Rica Dome. (Source: Fiedler 2002)

The subsequent intensification of the El Niño current brings increased rainfall to the arid regions along the coasts of southern Ecuador and northern Peru, and the increase in SSTs causes mortalities of cold-water marine fishes and birds (Sverdrup *et al.* 1942). An extensive presentation of the dynamics and impacts of El Niño events in the Atlantic, Indian, and Pacific Oceans may be found in *El Niño, La Niña, and the Southern Oscillation* (Philander 1990), and a collection of papers providing a

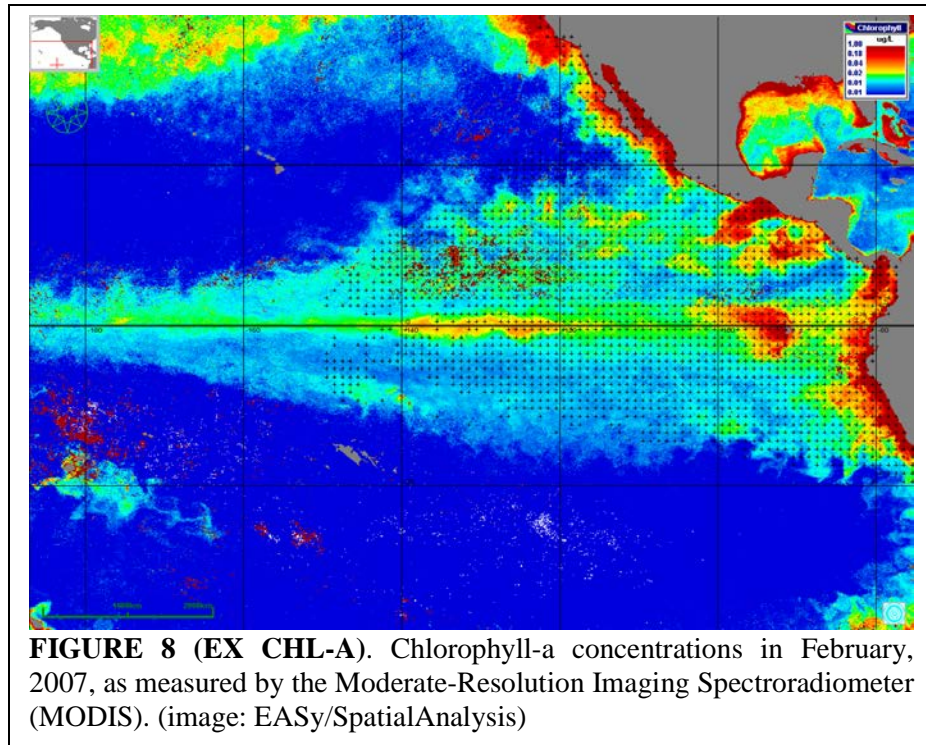


**FIGURE 8 (EX CHL-A).** Chlorophyll-a concentrations in February, 2007, as measured by the Moderate-Resolution Imaging Spectroradiometer (MODIS). (image: EASy/SpatialAnalysis)

more recent review focused on the EPO may be found in *Progress in Oceanography* (2006, Vol. 69).

The El Niño-Southern Oscillation (ENSO) refers to the state of multiple atmosphere-ocean feedback loops in which temperatures and flows in one system, *e.g.* the Walker circulation, causes a change in an ocean current, which then causes changes in the Hadley circulation (see below). How shifts between states are initiated is not well understood (Wang and Fiedler 2006): for example, the shift from El Niño to neutral or La Niña states may be due to a non-linear response to solar forcing (Amador *et al.* 2006) or to changes in atmosphere-ocean conditions caused by interactions with the Madden-Julian Oscillation (Weickmann 1991, Takayabu *et al.* 1999), short-period intense convection events that occur for about 10-20 days in the Indian Ocean, then rapidly shift to the western north Pacific, where they again persist for about 10-20 days (Weickmann 1991, Takayabu *et al.* 1999). Regardless, the essential nature of the ties between atmosphere and ocean are that “the maxima of the sea temperature in the eastern and central equatorial Pacific occur as a result of anomalous weakening of the trade winds of the Southern Hemisphere with inherent weakening of the equatorial upwelling” (Bjerknes 1969). Two atmospheric circulations, or cells, are important to the following discussion.

The driver of El Niño events is the Walker Circulation (Bjerknes 1969; [Figure 9](#)), a closed-loop air flow pattern, or cell, that connects a low-pressure center in the western Pacific to a high-pressure center in the eastern Pacific. Warm, moist air rises over the western Pacific; as it rises it cools, loses moisture, and begins to move to the east, and the air pressure falls in the western Pacific. Air from the east blows towards the low-pressure region that has been created in the western Pacific. These low-altitude westward blowing winds are the trade winds. The low humidity of these winds and solar heating of the sea results in high evaporation rates in the EPO, which create the warm, moist air moving to the western Pacific. At altitude over the EPO the cold, dry air from the west creates a high-pressure area, resulting in air flowing from altitude to the lower atmosphere, where it converges into the trade winds and completes the circulation. The greater the pressure difference between west and east, the greater the strength of the trade winds. When the Walker Circulation weakens, the trade winds weaken, and it is possible for an El Niño to form.

Hadley Circulation (Bjerknes 1966, see [Figure 2](#)) also influences the occurrence of El Niño events. As the north- and southeast trade winds blow towards the equator, they pick up moisture and heat from the ocean, and as they converge over the ITCZ, they create the rising portion of the Hadley Circulation. This rising air transports energy from the surface regions of the ITCZ to altitudes of about 15 km and northward to higher latitudes. When the trade winds weaken, the Hadley Circulation strengthens as SSTs increase due to the decrease in wind-driven evaporation rates; this further intensifies the Hadley Circulation, which results in a further weakening of the trade winds. The high levels of water vapor in the atmosphere

resulting from solar heating and associated increasing SSTs, and the absence of transport for this moisture to the west with the trade winds, results in increased rainfall over the latitudes of the ITCZ.

The Walker and Hadley Circulations interact in such a way that in neither is air moving in strict vertical planes. For example, the interaction in the EPO north of the ITCZ causes rising air in the Hadley Circulation to move eastward as it encounters the west-east flow of the Walker Circulation.

El Niños begin in the early months of the year, when the ITCZ, which is located over the center of the region of highest SSTs in the EPO, shifts to its southernmost latitude. Currents warm off southern

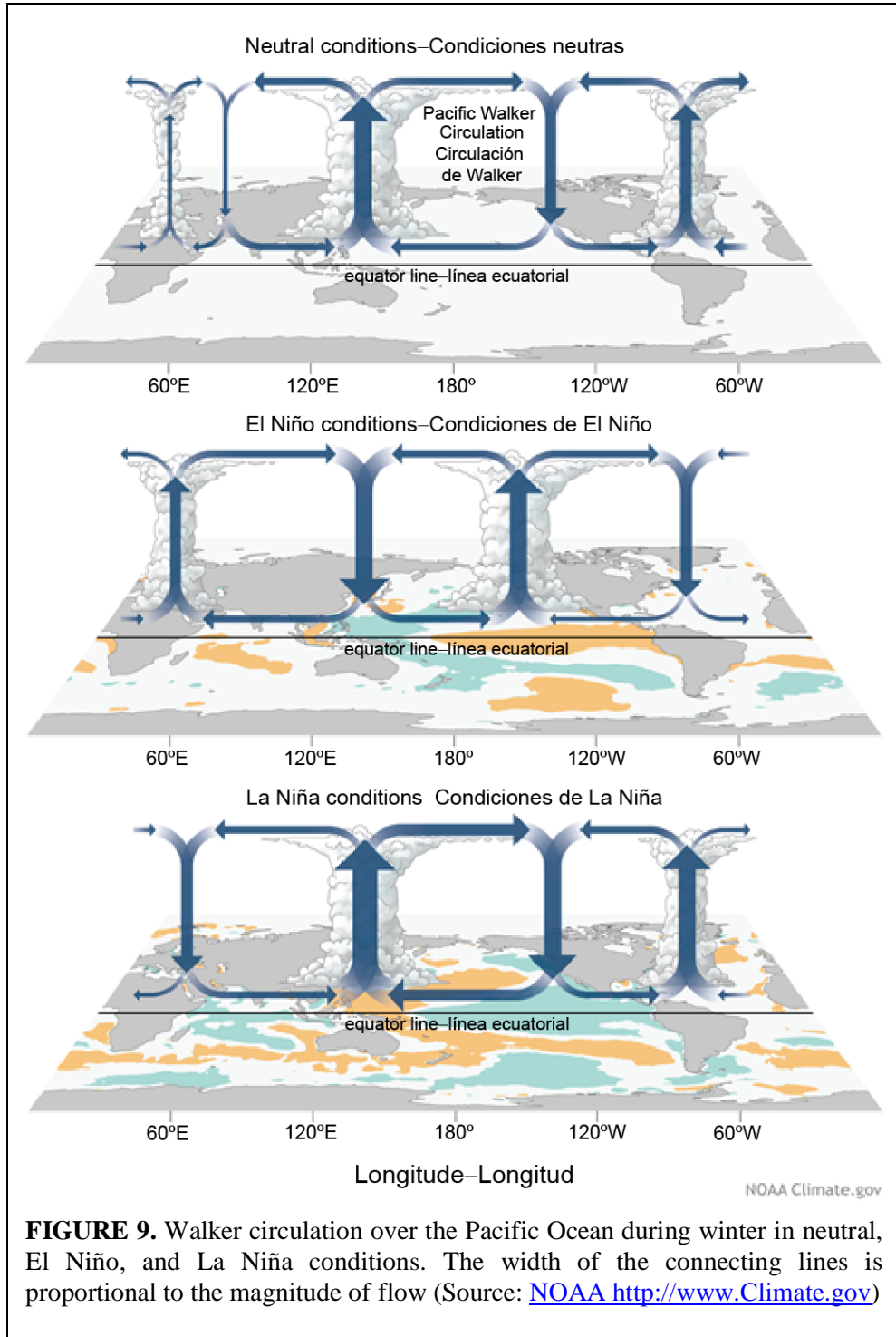


**FIGURE 9.** Walker circulation over the Pacific Ocean during winter in neutral, El Niño, and La Niña conditions. The width of the connecting lines is proportional to the magnitude of flow (Source: [NOAA http://www.Climate.gov](http://www.Climate.gov))

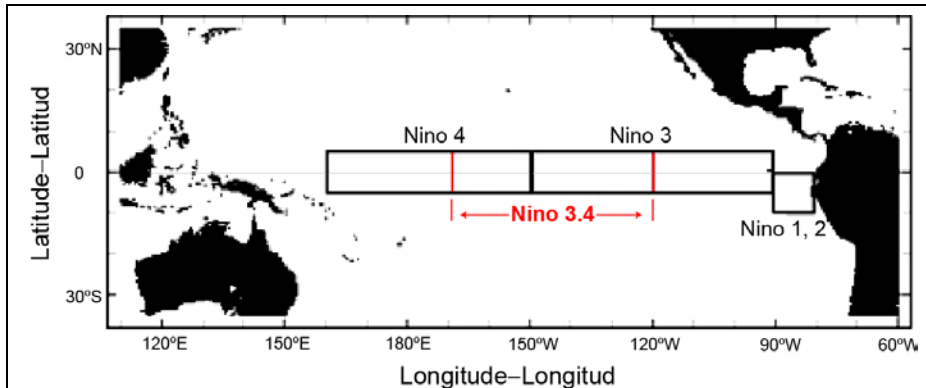


**FIGURE 10.** Regions within which monthly average SST is computed to provide indications of changes in state of El Niño-La Niña. Niño 3.4 was established to monitor the region at the interface of Ninos 3 and 4. (IRI, Columbia University, <http://iridl.ldeo.columbia.edu/maproom/ENSO/Diagnostics.html>)

Ecuador and northern Peru, and there is a further coincident weakening of the trade winds in the EPO. This weakening feeds back into decreased evaporation rates and a further weakening of the Walker Circulation. The decrease in cooling resulting from the lower evaporation rates leads to increased SSTs and expansion of the ITCZ to areas south of the equator. During some El Niños the ITCZ may

extend as far south as northern Peru, and it is the position and intensity of the ITCZ that often results in significant increases in precipitation in southern Ecuador and northern Peru.

The Southern Oscillation Index (SOI), long considered an indicator of El Niño events, is the standardized difference of the surface air pressure at Darwin, Australia, and at Tahiti, and provides a measure of the pressure difference driving Walker Circulation. The El Niño-Southern Oscillation (ENSO), the cycle between El Niño and La Niña, changes states as atmospheric pressure changes across the Pacific. During an El Niño the pressure in the western Pacific increases while that in the EPO decreases. The response is further weakening and possible reversal of the westward-flowing NEC and SEC, and a strengthening of the warm El Niño current flowing south along the coast of South America. There is also an increase in sea surface height (SSH) in the EPO and a decrease in the western Pacific as the warmer waters of the western central Pacific are advected into the EPO. The increase in SSH in the EPO causes a deepening of the thermocline, and the decrease in SSH in the western Pacific has the reverse effect in that region.

A number of indicators for ENSO<sup>1</sup> are used. Initially, four regions (Niño 1-4, [Figure 10](#)) were established in the equatorial Pacific for computing average SSTs. By 1996 research indicated that at times the conditions at the boundaries of areas 3 and 4 were informative, and area 3.4 was created<sup>2</sup>.

The Multivariate ENSO Index<sup>3</sup> (MEI) uses principal component analysis to combine sea-level pressure, zonal and meridional components of the surface winds, SST, surface air temperature, and cloud cover. This index incorporates the pressure information in the SOI and the SST information in the Niño 1-4 and Niño 3.4 regions, and adds information from direct measures of the key attributes observed in the atmosphere and ocean during El Niño and La Niña events. [Figure 11](#) shows the historical trend in the MEI, and [Figure 12](#) shows the strength of the developing 2015-2016 El Niño in comparison to previous weak El Niños. Another more recently developed index for identifying and describing El Niño events is the Trans-Niño Index (TNI), which is based on the differences in temperature between Niño 3.4 and Niño 1+2.

The purpose of the ENSO/El Niño indices is to give advance notice of coming changes in Pacific Ocean climate and to provide a means to describe and categorize observed El Niño/La Niña conditions. The usefulness of these indices for monitoring or managing fisheries depends on the accuracy and precision of

<sup>1</sup> <http://www.esrl.noaa.gov/psd/data/climateindices/list/>

<sup>2</sup> <http://www.cpc.ncep.noaa.gov/data/indices/Readme.index.shtml>

<sup>3</sup> <http://www.esrl.noaa.gov/psd/enso/mei/>

the indicators. Using the indices in fisheries management involves understanding the response of fleets and individual vessels to changes in local oceanographic conditions that influence fishing decisions. With such understanding, these indices may eventually provide something more than an indication that fishing will be better or worse from one year to the next (see [Section 3.](#)).

Vector fields of surface currents from the U.S. National Aeronautics and Space Administration Jet Propulsion Laboratory (NASA/JPL) high-resolution global ocean model for estimating the circulation and climate of the ocean (ECCO2) were used to estimate the path of currents during El Niño and La Niña events. The start and end points and pathlines for a one-month period are shown in [Figure 13](#). It is clear that at all stages of ENSO the pathlines move away from the equator. Those starting north of the equator move northward to about 8-10°N: those starting around 8-10°N move to the east-northeast, with those

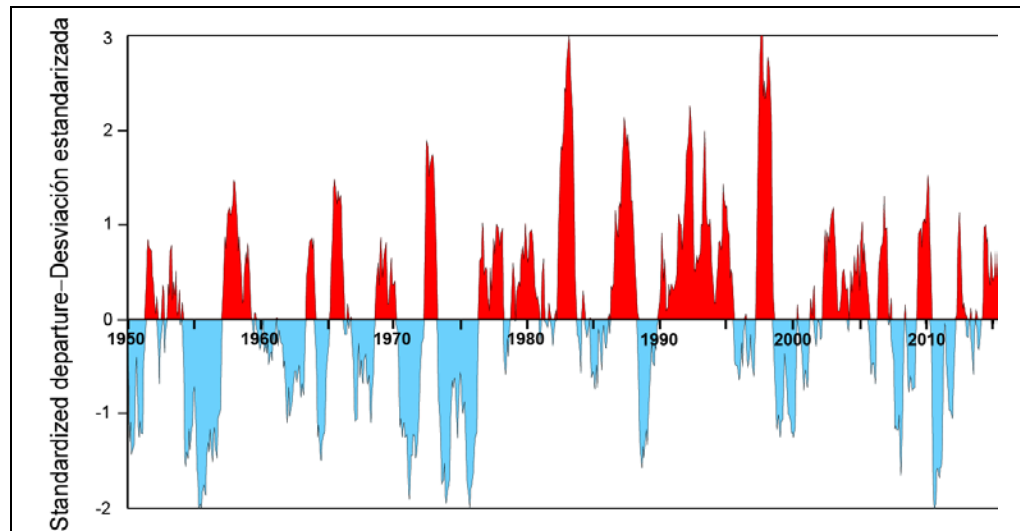


**FIGURE 11.** Trend of the Multivariate ENSO Index (MEI), 1950-2015.

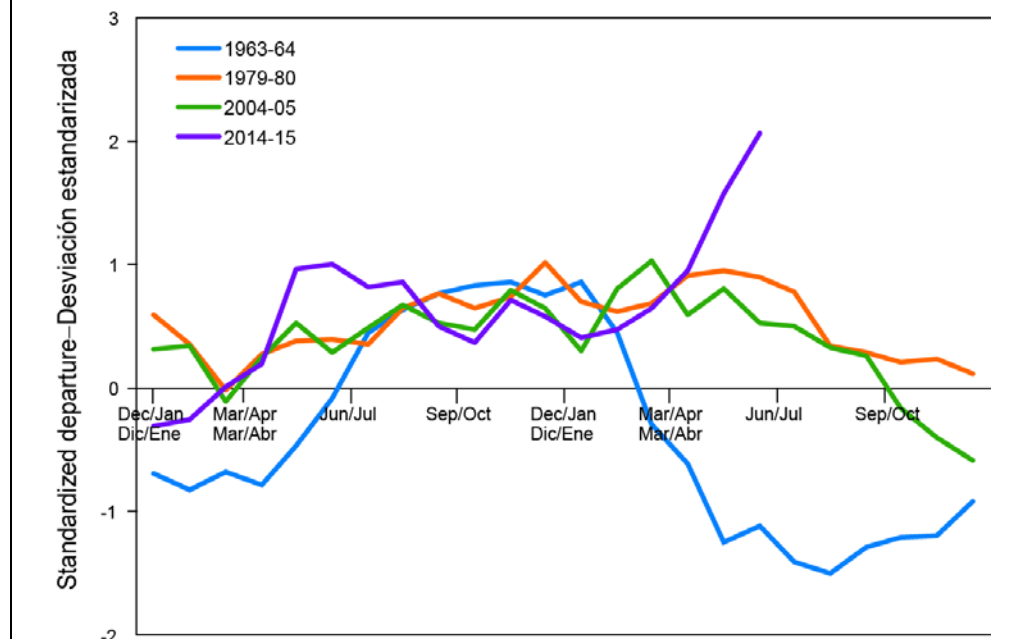


**FIGURE 12.** Comparison of the relative strength and timing of 2015 El Niño conditions to the temporal trend of monthly strength of three comparable weak El Niños. (<http://www.esrl.noaa.gov/psd/ensio/mei/-anomalies>)

near the northern reaches of the area breaking off to move northwesterly in the extension of the California Current/North Equatorial Current region. Those starting from locations near, but south of, the equator move west-southwest within the margins of the South Equatorial Current, while those south of the equator but closer to the South American continent move northward and then westward as they are entrained in the SEC. There is a striking difference between the vector fields for the two ENSO states: particularly evident is the

reversal of portions of the NEC and SEC. Such shifts in currents play a significant role in determining the location of fishing effort and the drift of fish-aggregating devices (FADs; see [Section 4](#)).

### 3. HISTORICAL TRENDS IN OCEANOGRAPHIC CONDITIONS

Data on atmospheric and ocean temperatures used to identify climate regime shifts have been available since the early 20<sup>th</sup> century. Climate regime shifts occurred in 1925, 1942, 1947, 1957, 1970, 1976-1977, and possibly 1998 (Graham 1994, Minobe 1997, Yasunaka and Hanawa 2005). A climate regime shift is a change from warmer(cooler) to cooler(warmer) climate; however, such shifts never return climate to exactly the previous state (Lorenz 1963). Climate regime shifts do not change long-term trends in global temperature, rather they are temporally-local changes in climate occurring on the (currently increasing) background trends in global temperature (Tsonis and Swanson 2012).

Climate regime shifts impact the timing and strength of El Niño events, and may also affect the factors that lead to such events. El Niño events that occur during warmer climate conditions are stronger, and last up to a year longer, than other El Niños (Yasunaka and Hanawa 2005). Since the 1976-1977 regime shift, the equatorial Pacific Ocean has been about 1.5°C warmer than before the shift (Stephens *et al.* 2001), and this warmer condition is conducive to the formation of, and stronger, El Niños. Regime shifts may also result in shifts in the events leading to El Niños.

Wang (1995) found that the 1976-1977 regime shift changed the nature of the forcing conditions leading to warming waters in the EPO and the development of El Niño events. Prior to the climate shift, such events followed large typhoons over northern Australia that led to warm waters propagating from the western Pacific into the EPO. This warming weakened the trade winds, and created conditions conducive to onset of an El Niño event. Since the 1976-1977 climate regime shift, the initiating typhoons have occurred over the Philippine Sea, and have increased the strength of the

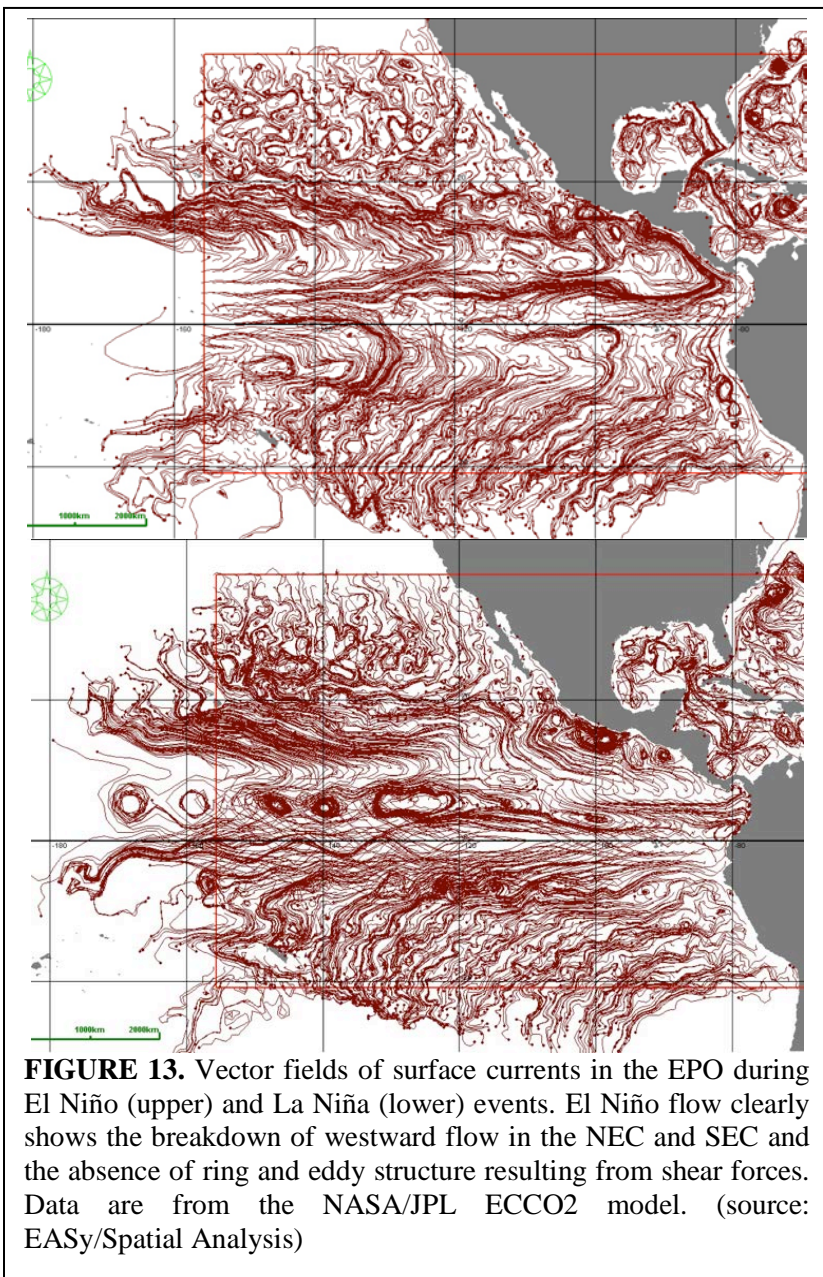
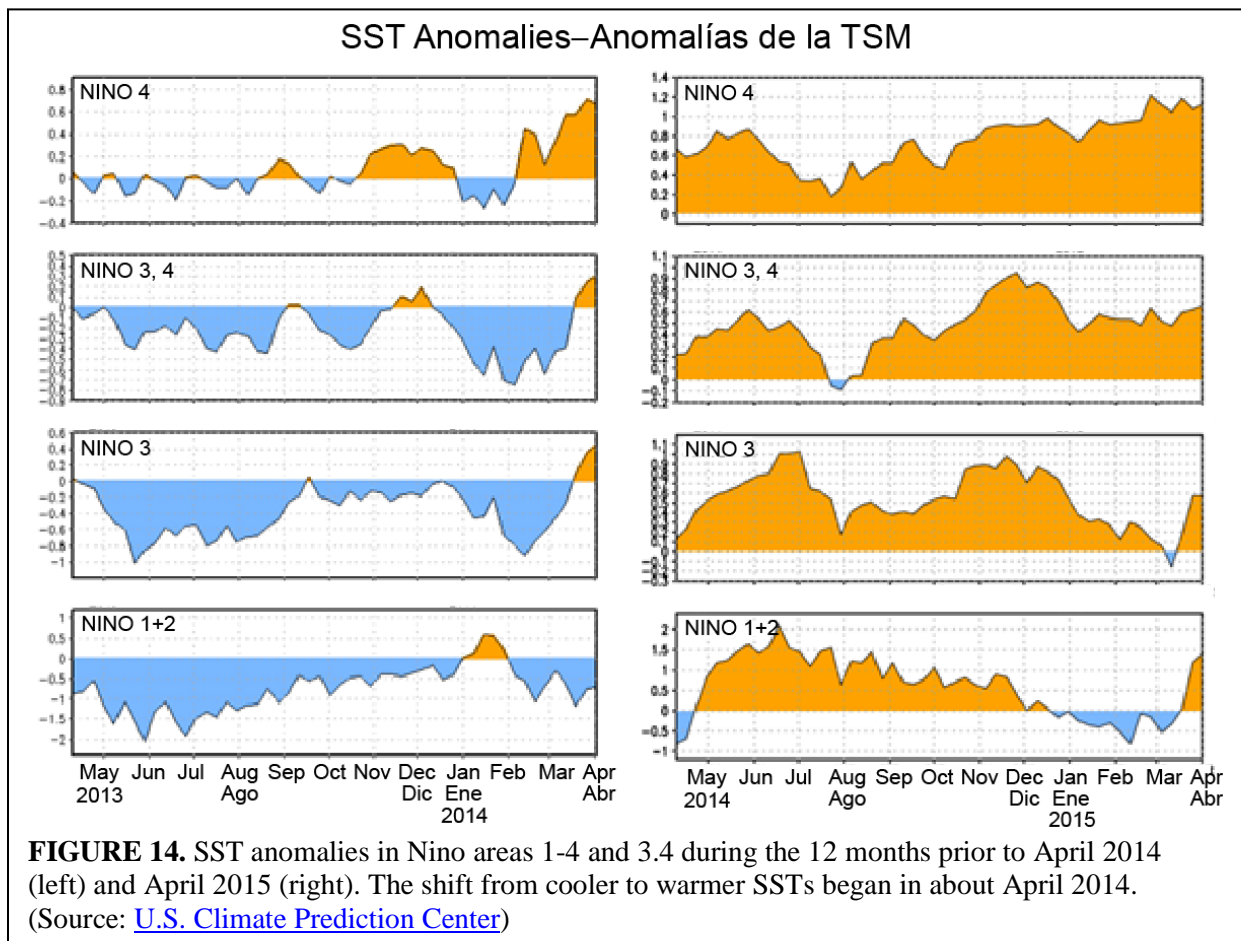


**FIGURE 13.** Vector fields of surface currents in the EPO during El Niño (upper) and La Niña (lower) events. El Niño flow clearly shows the breakdown of westward flow in the NEC and SEC and the absence of ring and eddy structure resulting from shear forces. Data are from the NASA/JPL ECCO2 model. (source: EASy/Spatial Analysis)

Westerlies and the southwest trade winds. These changes in the wind fields result in increased SSTs in the EPO, which are likewise conducive to El Niño events.

Cai *et al.* (2014) used coupled atmosphere-ocean models to examine the expected strength and frequency of El Niño events under conditions of global warming at levels similar to those observed previously. Their projections, based on the increased and increasing baseline temperatures of the EPO, indicated that the intensity and frequency of El Niño events increase with increases in baseline temperatures, because the decreased differential SSTs between the western and eastern Pacific allow more rapid and more intense warming of the EPO waters. The same could be expected following regime shifts to warmer conditions. These results are consistent with the conclusions of Yasunaka and Hanawa (2005). As climate and ocean models continue to improve, estimates and prediction of El Niño conditions should also improve.



The last strong El Niño occurred in 1997-1998. Since then there have been four more, in 2002-2003, 2004-2005, 2006-2007, and 2009-2010, and an extremely strong El Niño is forecast for 2015-2016. This is consistent with the greater frequency of occurrence (every 3-4 years) of El Niño since the last confirmed climate regime shift in 1976-1977.

#### 4. CURRENT AND PREDICTED OCEANOGRAPHIC CONDITIONS

In April 2015, weak El Niño conditions were evident in the EPO, with a 70 percent probability that they would continue through the boreal summer and a 60 percent probability that they would last through the

boreal fall<sup>4</sup>. The MEI showed that this El Niño had so far been comparable to the three weakest El Niños since 1950. An analysis of data from the Niño areas indicated that they were all experiencing SST anomalies of  $>0.5^{\circ}\text{C}$ . An El Niño event is defined as three consecutive months of positive anomalies at this level or greater. In addition, the SOI remained negative, another indication of an El Niño, and subsurface ocean temperatures increased significantly during the previous month. A comparison of the SST anomalies in the Niño areas during the 12 months up to April 2015 with those up to April 2014 is shown in [Figure 14](#).

In April 2014 the Pacific was in a neutral state that was expected to last through spring, with an increasing probability of El Niño conditions later in that year. In May the probability was only 50%, rising to 65% in June, but the year closed without El Niño conditions arising. By February 2015 the U.S. Climate Prediction Center was predicting a 50-60% chance of an El Niño in late winter or early spring, and in March 2015 a 50-60% chance that the El Niño that had started during the previous month would continue through summer 2015. At the time of writing (August 2015), what had been expected to be a relatively weak El Niño in 2015-2016 is now forecast to be one of the strongest on record ([Figure 12](#)).

## 5. OCEANOGRAPHIC IMPACTS ON TUNA STOCKS, FISHERIES, AND MANAGEMENT

Physical forcing of the ocean environment impacts all life stages of species taken in the EPO tuna fisheries. While changes in abundance have been observed at magnitudes similar to those resulting from fishing, the mechanisms by which forcing translates into such changes are generally unknown, but in analyses of population abundance they are the key to separating environmentally-induced changes from changes resulting from fishing (Rothschild 2015).

The spatial-temporal distributions of economically important or charismatic species are known with some certainty, and their response to ocean conditions has been the subject of research and a factor guiding the efforts of fishermen. The environmental parameter most often used in modeling population dynamics is temperature (Rothschild 2015), probably because of the ease of obtaining the data and of studying the effects of temperature on fish physiology and behavior.

Many studies of tunas have identified temperatures that are optimal for such as spawning, growth, and adult habitat, and also extremes which when exceeded result in mortalities, *e.g.* spending too much time diving in waters that are cold and also have a low concentration of dissolved oxygen. Spatial distributions of skipjack (*Katsuwonus pelamis*; SKJ) and yellowfin tunas are generally limited by the distribution of SSTs between about  $24^{\circ}$  and  $32^{\circ}\text{C}$  ([Figure 3](#)). These species also make regular dives to deeper waters to feed, but they are of limited duration: the synergistic effects of colder water and low dissolved oxygen concentrations (*e.g.* Barkley *et al.* 1978, Evans *et al.* 1981, Brill 1994, Schaefer *et al.* 2009) restrict their time spent at depth. Thermocline depth is easily monitored in real time, but that is not the case for the vertical distribution of oxygen concentrations. In the EPO, the top of the oxygen minimum layer is below, and closely associated with, the depth of the thermocline.

In purse-seine fisheries, variations in ocean parameters over space and time affect the spatial-temporal distributions of fishing effort. The direct effect of the distribution of these parameters may be increased fishing efficiency when nets extend into cooler waters with lower oxygen concentrations, because this could act as a barrier for tuna that would otherwise escape by diving out of the bottom of the net before it is pursued (*e.g.* Bane 1966). For reasons unknown, tunas, particularly skipjack, congregate under floating objects, including artificial fish-aggregating devices (FADs), and become available for capture with purse seines. An unexpected secondary impact of the introduction of FADs in the EPO in the 1990s resulted from the discovery that juvenile bigeye tuna (*Thunnus obesus*; BET) also schooled under the FADs, below the skipjack. The development of the FAD fishery caused a shift in the nature of the fishing effort by a large part of the fleet, with the locations of fishing for skipjack now being determined mainly by the

---

<sup>4</sup> U.S. National Weather Service  
[http://www.cpc.ncep.noaa.gov/products/analysis\\_monitoring/enso\\_advisory/ensodisc.pdf](http://www.cpc.ncep.noaa.gov/products/analysis_monitoring/enso_advisory/ensodisc.pdf)

drift of FADs across the EPO. Fishermen use their knowledge of current systems, combined with electronic devices that measure various oceanographic parameters, when deciding where to search for tunas and where to place FADs.

The longline fisheries of the EPO principally target bigeye, which are better able to control their body temperature. Their higher capacity for thermoregulation allows them to exploit the waters above the thermocline and to spend extended periods of time feeding below it during daylight hours (Schaefer and Fuller 2002). As a result, the fishing efficiency of longline gear that places hooks below the thermocline during the day is increased relative to gear that fishes at shallower depths. Here, too, oceanographic conditions affect the efficiency of fishing gear based on its configuration and operational characteristics, and allow fishermen to target their effort more effectively, maximizing the catch of target species and potentially avoiding bycatch of others.

Subsurface current structure impacts both purse-seine and longline fisheries. Current shear, which results from the friction between two currents that are in contact but are not moving in the same direction or at the same speed, creates turbulence along the interface. When purse seines or longlines are set where there are counter-flowing currents and shear, the gears do not operate as designed. Purse-seine nets tend to collapse inwards, with resulting loss of ability to purse the net or to easily brail the catch and bring it aboard the vessel. In the case of both purse seines and longlines, there is a tendency for the gear to reach the full set depth, to then shoal to the depth of the shear, and to then tangle if the turbulence is strong enough. These conditions also create uncertainty when standardizing longline fishing effort, since gear configuration is often used as a proxy for depth of fishing. In the presence of current shear, the gear configuration will not be consistent with expected depth of fishing, thus reducing the precision of the models and introducing bias. Examples of the impact of current shear on the depth of longline sets are shown in [Figure 15](#).

Oceanographic features in the central and eastern Pacific other than SST that are affected by El Niño conditions include thermocline depth, upwelling, and eddy and loop formation. Changes in these features may impact the recruitment and availability of tunas; for example, as the thermocline deepens, the availability and catchability of skipjack and yellowfin to the purse-seine fishery decreases, as do those of bigeye to the longline fishery.

Oceanographic conditions have significant impacts on the distributions of tunas, although the impacts are not necessarily consistent for all ages and/or species. For example, all three species (bigeye, skipjack, and yellowfin) spawn only in waters at or above 24°C, which suggests a physiological constraint limiting survival rates at some point in the early-life period of these species. As a result, the spatial-temporal distribution of spawners of these species is limited to equatorial regions east of 140-130°W in the boreal spring ([Figure 3](#)). During this period the optimum

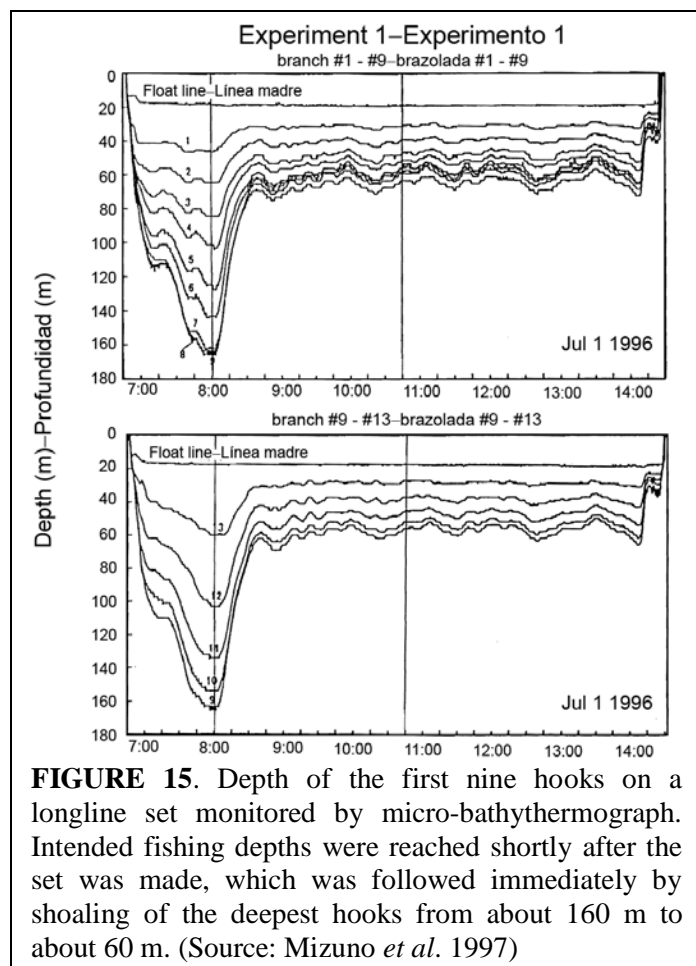


**FIGURE 15.** Depth of the first nine hooks on a longline set monitored by micro-bathythermograph. Intended fishing depths were reached shortly after the set was made, which was followed immediately by shoaling of the deepest hooks from about 160 m to about 60 m. (Source: Mizuno *et al.* 1997)

spawning regions (*i.e.*, those with SSTs >26°C) remain well separated both meridionally and zonally. This seasonal and spatial separation of regions suitable for spawning, which results from the distributions of physically-forced ocean conditions, affords a parsimonious explanation for including two cohorts in assessments of yellowfin (IATTC 1972), and also lends support to the hypothesis of at least two stocks (northern and southern) of yellowfin in the EPO.

Over the past half-century or so, much research has been dedicated to understanding the stock structure of tropical tunas and billfishes and, because the fisheries for tropical tunas are highly valuable economically, much of that research has focused on bigeye, skipjack, and yellowfin tunas. Schaefer (2008) reviewed and summarized key studies and findings from these decades of work; he found that no single factor determined stock structure, but that tagging experiments provided a key to understanding it for all three species. In the EPO, current flow fields act in a manner that contributes to the presence and continuing separation of populations in the northern and southern EPO, particularly those populations for which the distribution of early life stages may influence or determine locations of recruitment to juvenile and adult populations, after which relatively small ambits could maintain recruits relatively close to the locations where they were spawned.

This separation of stocks of yellowfin in the EPO is not unlike that for striped marlin (*Kajikia audax*, MLS) and swordfish (*Xiphias gladius*, SWO). The existence of discrete stocks of these two species in the EPO is supported by (1) analyses of oceanographic conditions, catch rates, archival tag data, and spatial and/or temporal separation of spawning regions (striped marlin: Gonzalez Armas *et al.* 1993, Gonzalez Armas *et al.* 1999, Domeier 2006, Hyde *et al.* 2006, Hinton 2009; swordfish: Claramunt and Herrera 1994, Hinton and Deriso 1994); (2) genetic analyses (striped marlin: Graves and McDowell 1994, McDowell and Graves 2008, Purcell 2009; swordfish: Alvarado Bremer *et al.* 2006, Lu *et al.* 2011); and (3) differences in life history parameters such as growth rates and maximum age and size-at-age distributions by region (Sun *et al.* 2002, Cerna 2009, Chong and Aguayo 2009). In the case of albacore tuna (*T. alalunga*, ALB), a highly migratory temperate-water species with distinct northern and southern stocks in the Pacific Ocean and age-specific but ecologically similar migration patterns in both hemispheres, the distributions of the two stocks mirror each other within similar environments of the central gyres. However, there is no indication that, perhaps as a result of temperature and/or lack of food, either stock crosses the equator at any time (Sund *et al.* 1981). All of these life history and biological parameters are functions of the conditions encountered by the fish in their oceanic habitat.

Knowing a species' preferences and limitations in terms of oceanographic characteristics makes it possible to target management measures to achieve the desired conservation goals for certain species, but at the same time not limit the catches of species for which there is no need for management.

Ocean bathymetry, a parameter that remains essentially constant over time, influences the presence of marine fauna. For example, a Taylor column over a seamount will tend to increase primary production in the area, and thus attract fish and marine mammals. The same is true of undersea ridges and islands, whose effects include shear zones, increased production, and aggregations of marine fauna. In the case of striped marlin in the southern Coral Sea, for example, spawning takes place in upwelling regions of the high seas associated with submarine ridges (Hanamoto 1972).

Pelagic marine species move to maintain favorable positions in their environments. In a study of the interaction of the Hawaiian longline fishery with protected sea turtles, Polovina *et al.* (2000) identified the SSTs and frontal regions of the northern Pacific in which these interactions were most likely to occur. Then, using information on the spatial-temporal distribution of oceanographic conditions, they identified specific closure periods and areas for the fishery that would prevent such interactions, thus allowing the fishery to continue operating.

Frequently, fisheries management involves restrictions on fishing within a specific area during a specific period, but the choice of areas and periods is not always based on scientific evidence. Hobday and Hartmann (2006) created a temperature-based habitat model for southern bluefin tuna (*Thunnus maccoyii*;

SBT) which integrated data on subsurface temperatures from a circulation model and satellite-derived measures of SST with ambient temperature data recorded by tags implanted in southern bluefin. The results led to a restructuring of management areas. In subsequent work, Hobday *et al.* (2010) improved the model so that it could be used to redefine closed areas during the fishing season, thus creating a dynamic habitat-based management model.

Estimating the abundance of a population for management purposes requires an index of abundance, and these are often modeled using data from the fisheries that capture the species being modeled. However, this requires that the effective effort of the fishing gear be determined; *i.e.* what proportion of the gear is actually fishing within the habitat of the target species. Some proposed solutions to this problem use models that include measures of preferred habitat (*e.g.* Hinton and Nakano 1996, Maunder *et al.* 2006, Valavanis *et al.* 2008, Su *et al.* 2011).

In the same manner, analyses of catch rates with oceanographic parameters may be used to direct fishing to highly productive areas. Among the many examples are analyses of skipjack fisheries and ocean parameters to improve fishing success (Andrade 2003, Oishi *et al.* 2006), of the relationship between oceanographic parameters and the distributions of prey species and skipjack with respect to upwelling conditions off Baja California (Blackburn 1970), and of variation in the recruitment of yellowfin due to variability in ocean parameters (Langley *et al.* 2009). Among the studies of north Pacific albacore, Polovina *et al.* (2001) and Zainuddin *et al.* (2004) used satellite-based measures of SST and primary production to identify migration and foraging regions along fronts in the north Pacific.

The current status of global warming has caused concern about the potential for changes in abundance and distribution of various marine species, including skipjack. The availability of large amounts of satellite-derived data and data from general circulation models provides the opportunity to model and consider these impacts (Loukos *et al.* 2003).

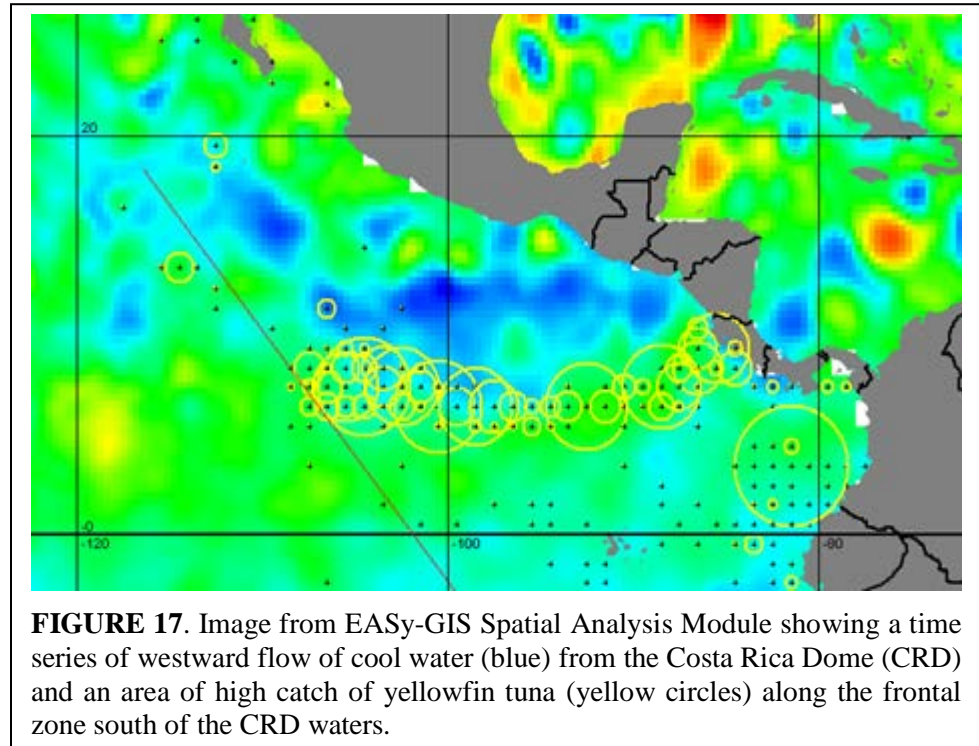
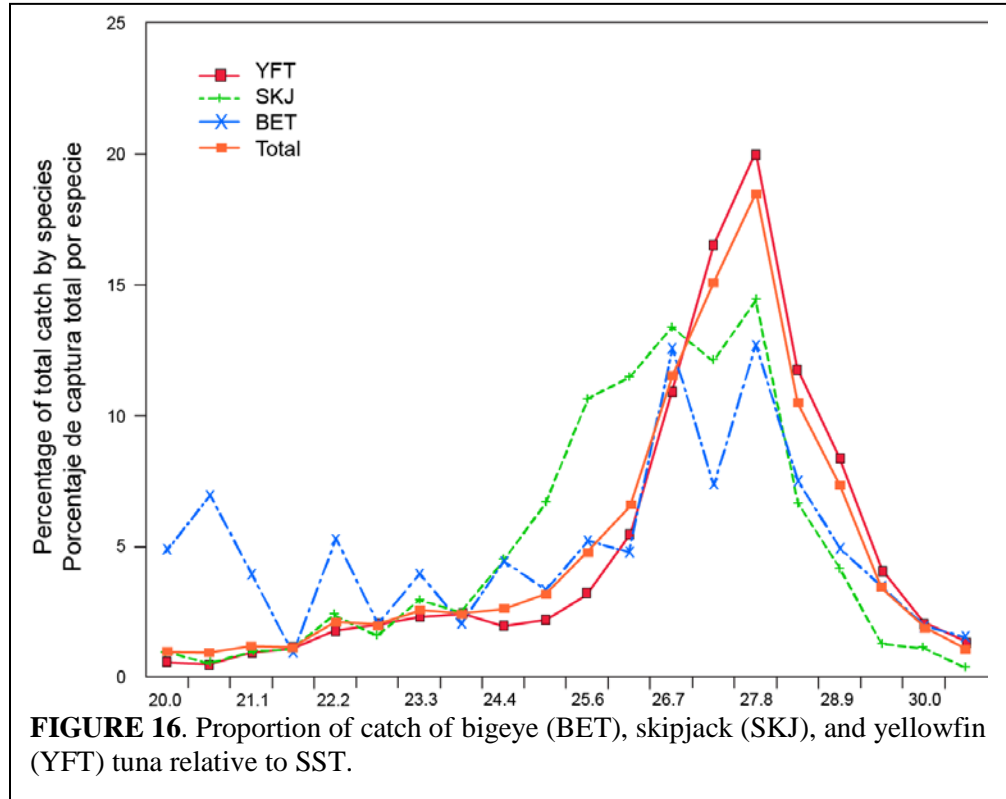
## **6. CURRENT RESEARCH**

Among the ongoing and planned research on fisheries oceanography and the EPO tuna fisheries are efforts to determine dynamic closure areas for the conservation of bigeye tuna, and to understand the response of the fishery to ocean variability, the oceanographic conditions affecting the dynamics of the fleet across states of ENSO, and the mechanisms driving recruitment of tunas in the EPO.

A key problem facing the purse-seine fisheries in the EPO is the catch of juvenile bigeye in sets on FADs. It is generally agreed that this catch should be reduced, but simply limiting or prohibiting sets on FADs would significantly reduce catches of skipjack, which are taken in great numbers in FAD sets throughout the Pacific.

Oceanographic conditions may provide a means to reduce catches of non-target species.

An analysis of the catches of bigeye, skipjack, and yellowfin with respect to the SST at the location and time of capture suggests that it may be possible to reduce catches of bigeye by restricting fishing to waters with SSTs above about 25°C (Figure 16). However, these preliminary results could be explained by other



hypotheses and parameters not yet examined, and more analyses are needed before the viability of this approach can be confirmed. It is worth noting in this context that the spatial-temporal distribution of cooler SSTs in the EPO is irregular and widespread, which might make management by area infeasible. However, with readily-available satellite-based small spatial-temporal scale measures of SST and the ability to

determine SST prior to making a set, the oceanographic parameter SST may possibly prove suitable for managing tuna and reducing bycatches in the EPO, while simultaneously minimizing the potential loss of catch of target species.

Satellite-based oceanographic data are among the key information needed to examine physical forcing and associations in large marine ecosystems and fisheries, but ready and easy access has been, and at times remains, problematic. Also, these data are developed for geophysical research, and are generally not available in formats commonly used in fisheries science.

The Spatial Analysis Module for the EASy-GIS<sup>5</sup> handles four-dimension arrays (X, Y, Z, T) to match, display, and conduct basic analyses of geophysical and fisheries data. Spatial Analysis can also call

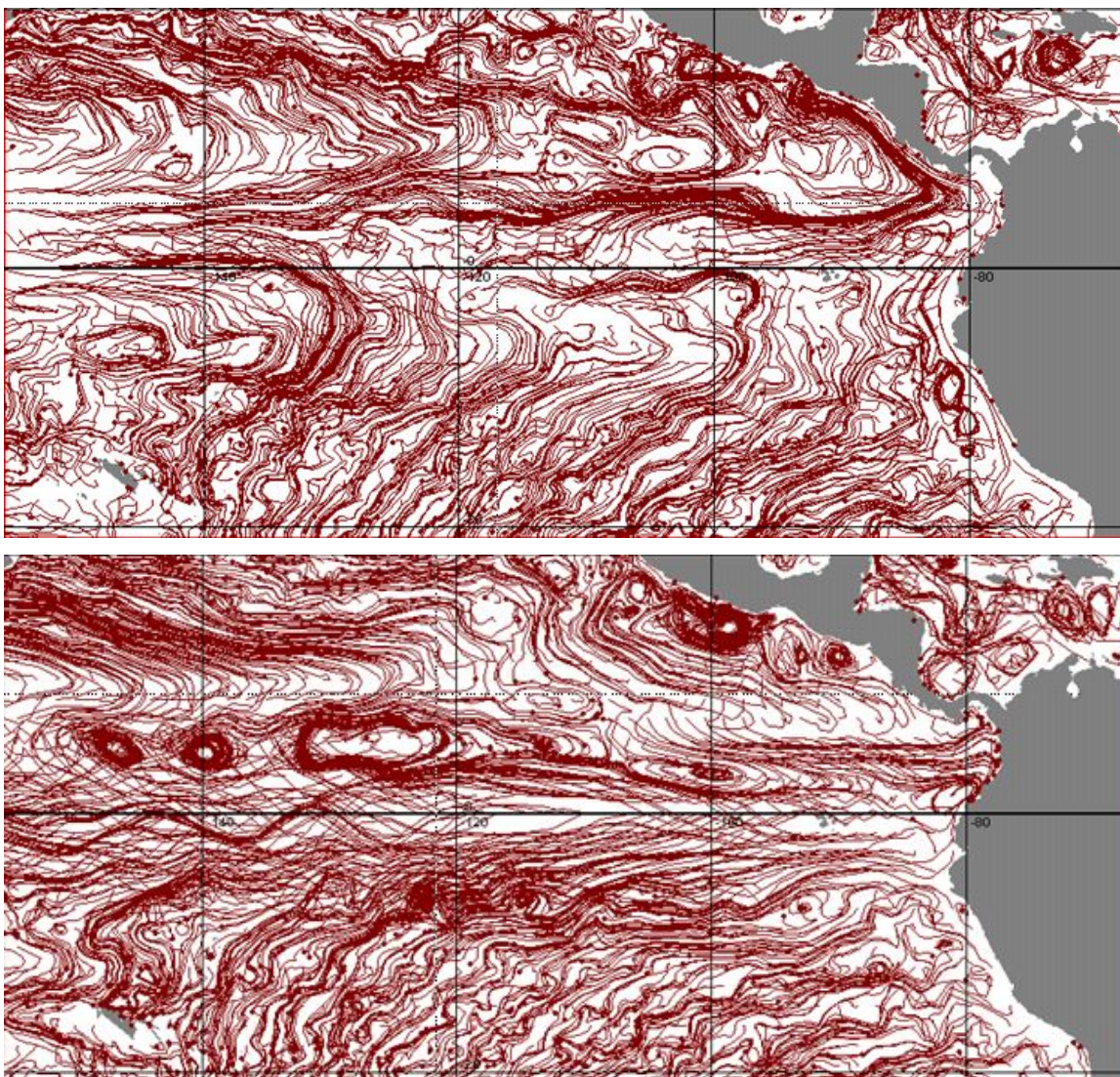


**FIGURE 18.** Large-scale current flow pathlines in the EPO between 20°N and 20°S during the 1997-1998 El Niño (upper panel) and the 1998-1999 La Niña (lower panel).

<sup>5</sup> Environmental Analysis System (EASy) Geographical Information System (GIS) for marine applications. [System Science Applications, Inc.](#)

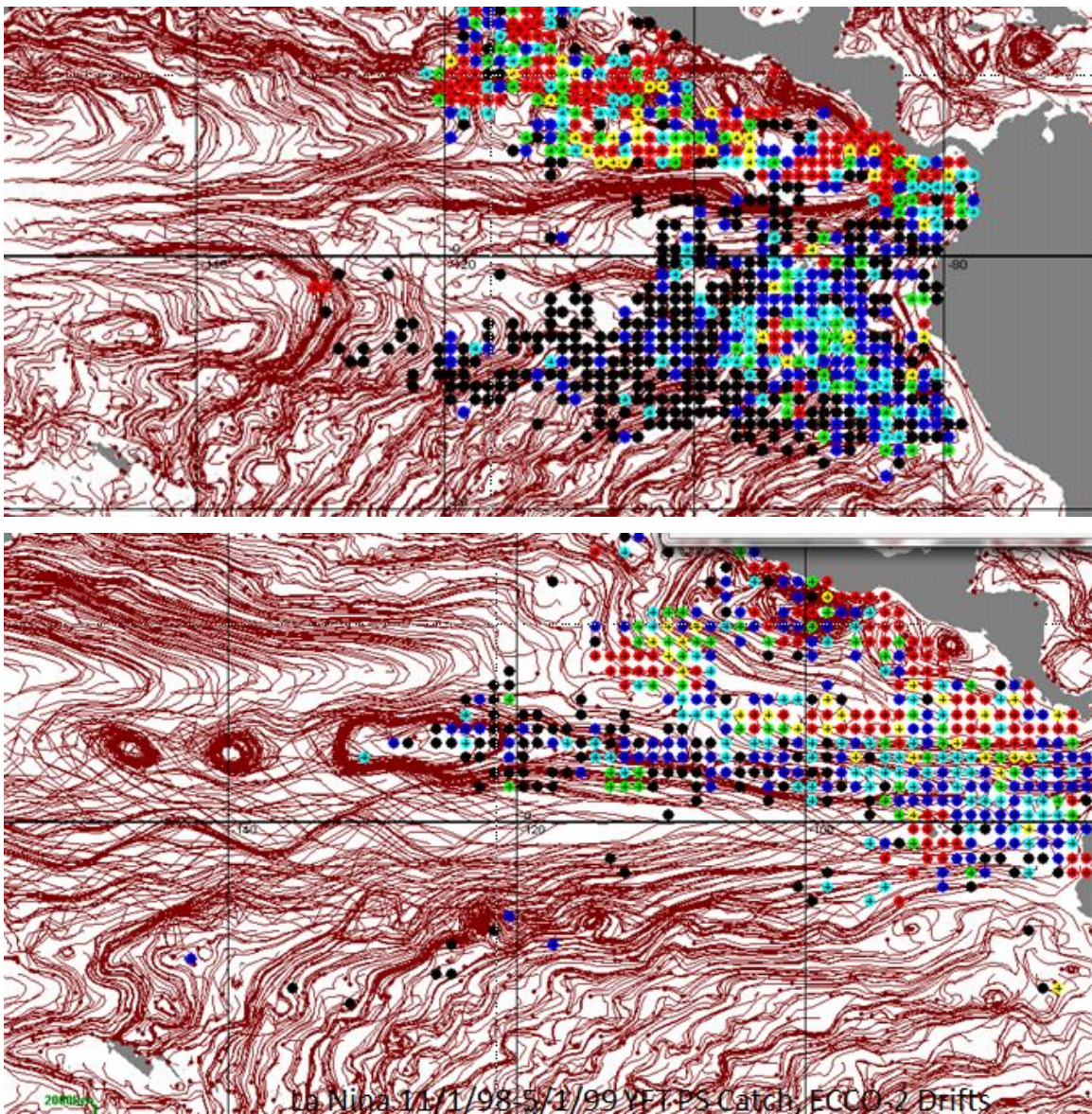


**FIGURE 19.** Locations of catches (low [black] to high [red]) of yellowfin in the EPO between 20°S and 20°N during the 1997-1998 El Niño (upper panel) and the 1998-1999 La Niña (lower panel).

procedures in R and export data files for subsequent analysis in programs such as ADMB, R, and SAS. The development of the module, and open access to the EASy-GIS system on which it runs, were made possible by a grant<sup>6</sup> from the United States National Aeronautics and Space Administration (NASA). The system and module are available without cost to users.

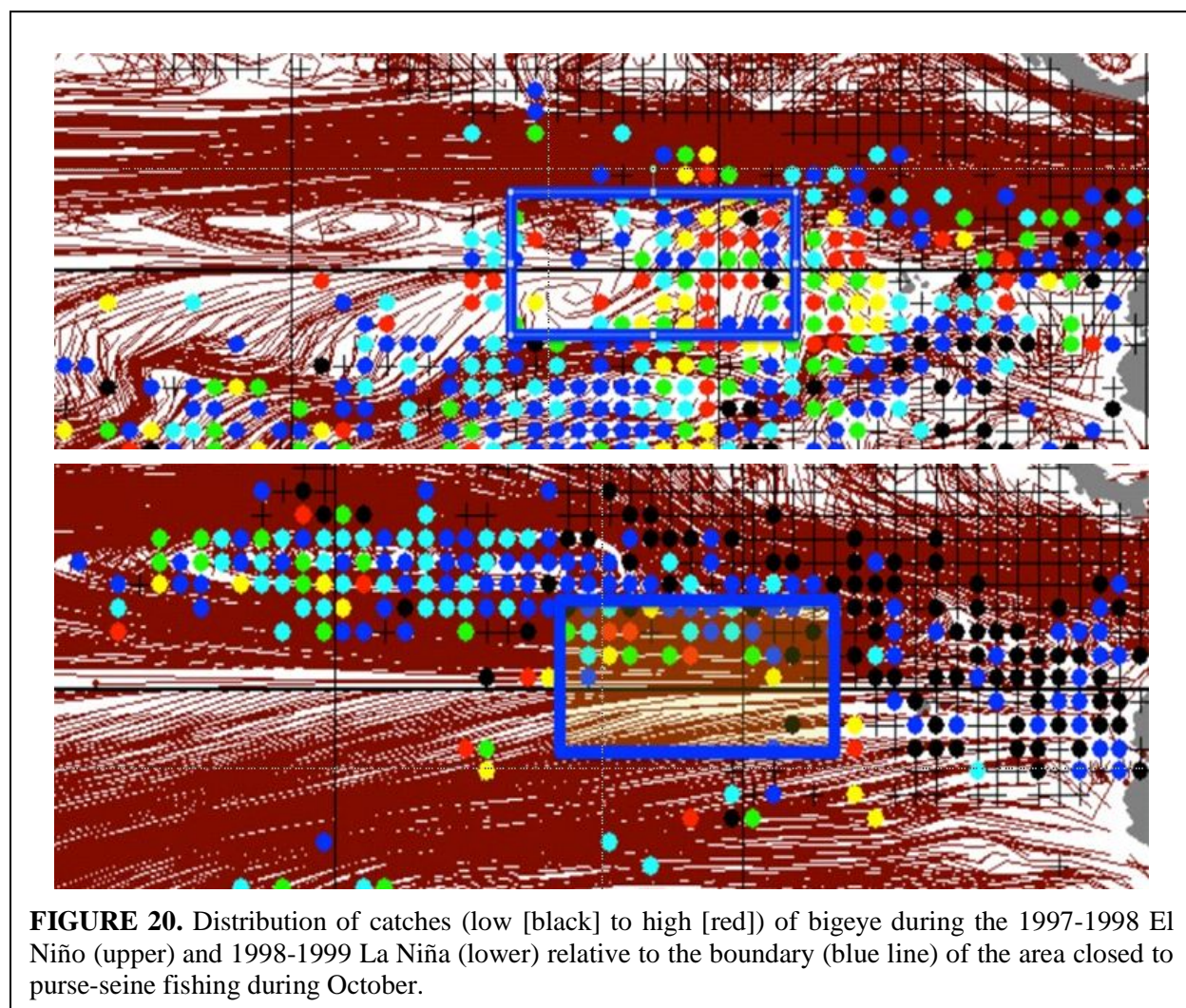
An example of the use of the module to examine the response of purse seiners to ocean characteristics is shown in [Figure 17](#). The catch of yellowfin over time corresponds with a frontal zone extending from coastal regions near the Costa Rica Dome along the westward-flowing extension of upwelled cooler water from the Dome.

<sup>6</sup> NASA [ROSES 2007](#) DSS-07

EASy-GIS provides a fully interactive means to run time series of fishing data overlaid by oceanographic data. [Figure 18](#) illustrates the significant difference in surface current patterns during a strong El Niño (1997-1998) and subsequent La Niña (1998-1999). The spatial-temporal distribution of fishing effort responds to shifts in such current patterns and in the distributions of oceanographic conditions ([Figure 19](#)).

The ability to model ocean and fisheries data together makes it possible to provide improved management advice and options that take these ocean-fishery relationships into account. The shift of fishing effort with respect to the closure area adopted in IATTC conservation resolutions is shown in [Figure 20](#).

Fishermen take oceanographic conditions into account when deciding on their fishing strategies, and many now make use of commercial products<sup>7</sup> that provide current analyses of ocean conditions based on satellite data such as surface and sub-surface temperatures, mixed layer depth, and weather. Given the response of vessels to changing oceanographic conditions, including oceanographic parameters in models of fishing vessel operations should improve the ability to project the distributions of fleets and their



responses to changes in the environment and fisheries management. In a study<sup>8</sup> funded by the United

<sup>7</sup> e.g. SeaView [http://www.oceani.com/Services\\_SeaView.html](http://www.oceani.com/Services_SeaView.html)

<sup>8</sup> Fishscape: <https://www.collectiveip.com/grants/NSF:1010280>

States National Science Foundation, ocean parameters were included in a model<sup>9</sup> of fleet dynamics of the EPO tuna fisheries. The model projects the operations of individual vessels based on their current operational status, such as fuel on board and tons of fish on board, and on the ocean environment at the vessel's current position and at alternative fishing locations that it has "under consideration".

## 7. SUMMARY

The principal zonal surface currents in the EPO are wind-driven and are (from north to south) the westward-flowing North Equatorial Current, the eastward-flowing North Equatorial Countercurrent, and the westward-flowing South Equatorial Current. The eastward-flowing subsurface Equatorial Undercurrent is centered on the equator. The dynamics of these currents, and of those they feed in the EPO, are not well known. The California and the Humboldt eastern boundary currents contribute significant flow into the North and South Equatorial Currents.

The interannual climate of the region is dominated by the El Niño-Southern Oscillation (ENSO), which shifts between states about every five years, although the frequency has been decreasing in the recent past. Regime shifts that change the baseline temperatures of the region occur at intervals of about 15-25 years, and in the equatorial Pacific they affect the frequency and intensity of El Niño events. The regime shift in 1976-1977 increased equatorial SSTs by about 1.5°C. Over time, the increasing accuracy and precision of integrated global atmosphere-ocean models will improve the ability to predict shifts in state of the ENSO.

The EPO covers about 18 percent of the surface area of the oceans, but it produces about 22 percent of the global primary production. Primary production occurs throughout the EPO, although, due to the shallow thermocline over the region resulting in a compressed euphotic zone, most production is from microplankton. High chlorophyll-a concentrations and levels of production are evident near the continent and along the equator, where upwelling provides input of iron, the limiting factor for primary production in the EPO.

Fisheries oceanography provides a means of increasing production from fisheries, reducing bycatch, and developing management options for regulated fisheries. It has proven effective in standardizing catch rates for use in stock assessments and in developing dynamic management options for highly migratory species, such as those developed for southern bluefin tuna. It is expected to increase options for managing tunas in the EPO and for reducing bycatch.

Understanding fleet dynamics and movements as ocean conditions change is important to fisheries assessment and to fisheries management. In stock assessments and development of management recommendations, assumptions must be made about fleet response and redistribution of fishing effort in response to external controls. Oceanographic parameters have been included in an integrated EPO tuna fisheries model that includes ocean conditions, stock production, fishing fleet dynamics, and impacts of management. The significant response of the fleet to El Niño/La Niña conditions has been identified, which will make it possible to consider options for management actions in the face of environmental change.

With information on limiting and preferred temperatures for tunas, it has been possible to identify the spatial-temporal distribution of waters suitable for spawning and for adult tunas. Understanding of oceanographic conditions has also contributed to the delineation, confirmed by genetic data analyses, of stock structure of the tunas and billfishes of the EPO.

## 8. LITERATURE CITED

Alvarado Bremer, J. R., M. G. Hinton and T. W. Greig (2006). Evidence of spatial genetic heterogeneity in Pacific swordfish (*Xiphias gladius*) revealed by the analysis of *ldh-A* sequences. [Bulletin of](#)

---

<sup>9</sup> Sun, J., M.G. Hinton, & D.G. Webster. 2015. Modelling the Spatial Dynamics of International Tuna Fleets. Submitted to Plos One ([www.plosone.org](http://www.plosone.org)).

- [Marine Science](#) **79**(3): 493–503.
- Amador, J. A., E. J. Alfaro, O. G. Lizano and V. O. Magaña (2006). Atmospheric forcing of the eastern tropical Pacific: A review. [Progress in Oceanography](#) **69**(2–4): 101-142.
- Andrade, H. A. (2003). The relationship between the skipjack tuna (*Katsuwonus pelamis*) fishery and seasonal temperature variability in the south-western Atlantic. [Fisheries Oceanography](#) **12**(1): 10-18.
- Bane, G. W., Jr. (1966). Hydrography and the yellowfin tuna, *Thunnus albacares*, in the Gulf of Guinea. [Ghana Journal of Science](#) **6**: 115-137.
- Barkley, R. A., W. H. Neill and R. M. Gooding (1978). Skipjack tuna, *Katsuwonus pelamis*, habitat based on temperature and oxygen requirements. [Fishery Bulletin](#) **76**(3): 653-662.
- Bjerknes, J. (1966). A possible response of atmospheric Hadley Circulation to equatorial anomalies of ocean temperature. [Tellus](#) **18**(4): 820-829.
- Bjerknes, J. (1969). Atmospheric teleconnections from equatorial Pacific. [Monthly Weather Review](#) **97**(3): 163-172.
- Blackburn, M. (1970). Conditions related to upwelling which determine distribution of tropical tunas off western Baja California. [United States Fish and Wildlife Service Fishery Bulletin](#) **68**(1): 147-&.
- Brill, R. W. (1994). A review of temperature and oxygen tolerance studies of tunas pertinent to fisheries oceanography, movement models and stock assessments. [Fisheries Oceanography](#) **3**(3): 204-216.
- Cai, W., S. Borlace, M. Lengaigne, P. van Rensch, M. Collins, G. Vecchi, A. Timmermann, A. Santoso, M. J. McPhaden, L. Wu, M. H. England, G. Wang, E. Guilyardi, and F.-F. Jin. (2014). Increasing frequency of extreme El Nino events due to greenhouse warming. [Nature Climate Change](#) **4**(2): 111-116.
- Cerna, J. F. (2009). Age and growth of the swordfish (*Xiphias gladius* Linnaeus, 1758) in the southeastern Pacific off Chile (2001). [Latin American Journal of Aquatic Research](#) **37**(1): 59-69.
- Chong, J. and M. Aguayo (2009). Age and growth of swordfish (*Xiphias gladius* Linnaeus, 1758) in the southeastern Pacific (December 1994-September 1996). [Latin American Journal of Aquatic Research](#) **37**(1): 1-15.
- Claramunt, G. and G. Herrera (1994). A new method to estimate the fraction of daily spawning females and the numbers of spawnings in *Sardinops sagax* in northern Chile. [Scientia Marina](#) **58**(3): 169-177.
- Cromwell, T. (1958). Thermocline topography, horizontal currents and ridging in the eastern tropical Pacific. [Bulletin of the Inter-American Tropical Tuna Commission](#) **3**: 135-164.
- Domeier, M. L. (2006). An analysis of Pacific striped marlin (*Tetrapturus audax*) horizontal movement patterns using pop-up satellite archival tags. [Bulletin of Marine Science](#) **79**(3): 811-825.
- Evans, R. H., D. R. McLain and R. A. Bauer (1981). Atlantic skipjack tuna: influences of mean environmental conditions on their vulnerability to surface fishing gear. [Marine Fisheries Review](#) **43**(6): 1-11.
- Fiedler, P. C. (2002). The annual cycle and biological effects of the Costa Rica Dome. [Deep-Sea Research Part I-Oceanographic Research Papers](#) **49**(2): 321-338.
- Gonzalez Armas, R., R. Funes Rodriguez and V. A. Levy Perez (1993). First record of *Tetrapturus audax* larvae (Scombroidei: Istiophoridae) in the coast of Jalisco, eastern Pacific of Mexico. [Revista de biologia tropical. San Jose](#) **41**(3-B): 919-920.
- Gonzalez Armas, R., O. Sosa-Nishizaki, R. Funes Rodriguez and V. A. Levy Perez (1999). Confirmation of the spawning area of the striped marlin, *Tetrapturus audax*, in the so-called core area of the eastern tropical Pacific off Mexico. [Fisheries Oceanography](#) **8**(3): 238-242.
- Graham, N. E. (1994). Decadal-scale climate variability in the tropical and north Pacific during the 1970s and 1980s: observations and model results. [Climate Dynamics](#) **10**(3): 135-162
- Graves, J. E. and J. R. McDowell (1994). Genetic analysis of striped marlin (*Tetrapturus audax*)

- population structure in the Pacific Ocean. Canadian Journal of Fisheries and Aquatic Sciences **51**: 1762-1768.
- Hanamoto, E. (1972). Fishery oceanography of striped marlin. 2. Spawning activity of the fish in the southern Coral Sea. Bulletin of the Japanese Society of Scientific Fisheries **43**(11): 1279-1286.
- Hinton, M. G. (2009). Considerations on regions for use in stock assessments of striped marlin. ISC Billfish Working Group. Honolulu, Hawaii, USA, International Scientific Committee for Tuna and Tuna-like Species in the North Pacific Ocean. ISC/09/BILLWG-1: 7.
- Hinton, M. G. and R. B. Deriso (1994). Distribution and stock assessment of swordfish, *Xiphias gladius*, in the eastern Pacific Ocean from catch and effort data standardized on biological and environmental parameters. Biology and fisheries of swordfish, *Xiphias gladius*, Ensenada, B.C., Mexico, U.S. Department of Commerce.
- Hinton, M. G. and H. Nakano (1996). Standardizing catch and effort statistics using physiological, ecological, or behavioral constraints and environmental data, with an application to blue marlin (*Makaira nigricans*) catch and effort data from Japanese longline fisheries in the Pacific. Bulletin of the Inter-American Tropical Tuna Commission **21**(4): 169-200.
- Hobday, A. J. and K. Hartmann (2006). Near real-time spatial management based on habitat predictions for a longline bycatch species. Fisheries Management and Ecology **13**(6): 365-380.
- Hobday, A. J., J. R. Hartog, T. Timmiss and J. Fielding (2010). Dynamic spatial zoning to manage southern bluefin tuna (*Thunnus maccoyii*) capture in a multi-species longline fishery. Fisheries Oceanography **19**(3): 243-253.
- Hyde, J. R., R. Humphreys, M. Musyl, E. Lynn and R. Vetter (2006). A central north Pacific spawning ground for striped marlin, *Tetrapturus audax*. Bulletin of Marine Science **79**(3): 683-690.
- IATTC (1972). Annual report of the Inter-American Tropical Tuna Commission 1971. La Jolla, California, USA, Inter-American Tropical Tuna Commission: 129 p.
- Langley, A., K. Briand, D. S. Kirby and R. Murtugudde (2009). Influence of oceanographic variability on recruitment of yellowfin tuna (*Thunnus albacares*) in the western and central Pacific Ocean. Canadian Journal of Fisheries and Aquatic Sciences **66**(9): 1462-1477.
- Lorenz, E. N. (1963). Deterministic non-periodic flow. Journal of the Atmospheric Sciences **20**(2): 130-141
- Loukos, H., P. Monfray, L. Bopp and P. Lehodey (2003). Potential changes in skipjack tuna (*Katsuwonus pelamis*) habitat from a global warming scenario: modelling approach and preliminary results. Fisheries Oceanography **12**(4-5): 474-482.
- Lu, C. P., B. L. Smith, M. G. Hinton and J. R. Alvarado Bremer (2011). Population structure study of swordfish *Xiphias gladius* in the Pacific Ocean inferred by genetic informative data differentiation using High Resolution Melting Analysis (HRMA). American Fisheries Society 141st Annual Meeting. Seattle, WA.
- Maunder, M. N., M. G. Hinton, K. A. Bigelow and A. D. Langley (2006). Developing indices of abundance using habitat data in a statistical framework. Bulletin of Marine Science **79**(3): 545-559.
- McDowell, J. R. and J. E. Graves (2008). Population structure of striped marlin (*Kajikia audax*) in the Pacific Ocean based on analysis of microsatellite and mitochondrial DNA. Canadian Journal of Fisheries and Aquatic Sciences **65**(7): 1307-1320.
- Minobe, S. (1997). A 50-70 year climate oscillation over the North Pacific and North America. Geophysical Research Letters **24**(6): 683-686.
- Mizuno, K., M. Okazaki, H. Nakano and H. Okamura. (1997). Estimation of underwater shape of tuna longline by using micro-BTs. Bulletin of the National Research Institute of Far Seas Fisheries **34**: 1-24.
- Oishi, K., A. Nihira, T. Kuroyama and S. I. Saitoh (2006). Predictable hotspots for skipjack tuna,

- (*Katsuwonus pelamis*), using multi-sensor satellite remote sensing off the east coast of Japan, North Pacific Marine Science Organization (PICES), P.O. Box 6000 Sidney B.C. V8L 4B2 Canada.
- Pennington, J. T., K. L. Mahoney, V. S. Kuwahara, D. D. Kolber, R. Calienes and F. P. Chavez (2006). Primary production in the eastern tropical Pacific: A review. Progress in Oceanography **69**(2-4): 285-317.
- Philander, S. G. (1990). El Nino, La Nina and the Southern Oscillation. San Diego, Academic Press.
- Polovina, J. J., E. Howell, D. R. Kobayashi and M. P. Seki (2001). The transition zone chlorophyll front, a dynamic global feature defining migration and forage habitat for marine resources. Progress in Oceanography **49**(1-4): 469-483.
- Polovina, J. J., D. R. Kobayashi, D. M. Parker, M. P. Seki and G. R. Balazs (2000). Turtles on the edge: movement of loggerhead turtles (*Caretta caretta*) along oceanic fronts, spanning longline fishing grounds in the central North Pacific, 1997-1998. Fisheries Oceanography **9**(1): 71-82.
- Purcell, C. M. (2009). Genetic Analysis of Population Structure in Striped Marlin, *Tetrapturus audax*, in the Pacific Ocean. Ph.D., University of Southern California.
- Ren, H. L. and F. F. Jin (2011). Nino indices for two types of ENSO. Geophysical Research Letters **38**.
- Rothschild, B. J. (2015). On the birth and death of ideas in marine science. ICES Journal of Marine Science: 8.
- Schaefer, K. M. (2008). Stock structure of bigeye, yellowfin and skipjack tunas in the eastern Pacific Ocean. Stock Assessment Report. Inter-American Tropical Tuna Commission. Inter-American Tropical Tuna Commission. **9**: 203-221.
- Schaefer, K. M. and D. W. Fuller (2002). Movements, behavior, and habitat selection of bigeye tuna (*Thunnus obesus*) in the eastern equatorial Pacific, ascertained through archival tags. Fishery Bulletin **100**(4): 765-788.
- Schaefer, K. M., D. W. Fuller and B. A. Block (2009). Vertical movements and habitat utilization of skipjack (*Katsuwonus pelamis*), yellowfin (*Thunnus albacares*), and bigeye (*Thunnus obesus*) tunas in the equatorial eastern Pacific Ocean, ascertained through archival tag data. Tagging and Tracking of Marine Animals with Electronic Devices. J. L. Nielsen, H. Arrizabalaga, N. Fragoso *et al.*, Springer. **9**: 121-144.
- Stephens, C., S. Levitus, J. Antonov and T. P. Boyer (2001). On the Pacific Ocean regime shift. Geophysical Research Letters **28**(19): 3721-3724.
- Su, N.-J., C.-L. Sun, A. E. Punt, S.-Z. Yeh and G. Dinardo (2011). Evaluation of a spatially sex-specific assessment method incorporating a habitat preference model for blue marlin (*Makaira nigricans*) in the Pacific Ocean. Fisheries Oceanography **20**(5): 415-433.
- Sun, C. L., S. P. Wang and S. Z. Yeh (2002). Age and growth of the swordfish (*Xiphias gladius* L.) in the waters around Taiwan determined from anal-fin rays. Fishery Bulletin **100**(4): 822-835.
- Sund, P. N., M. Blackburn and F. Williams. (1981). Tunas and their environment in the Pacific Ocean: a review. Oceanography and Marine Biology, an Annual Review **19**: 443-512.
- Svedrup, H. U., M. W. Johnson and R. H. Fleming (1942). The Oceans: Their Physics, Chemistry, and General Biology. New York, Prentice Hall, Inc.
- Takayabu, Y. N., T. Iguchi, M. Kachi, A. Shibata and H. Kanzawa (1999). Abrupt termination of the 1997-98 El Nino in response to a Madden-Julian oscillation. Nature **402**(6759): 279-282.
- Tsonis, A. A. and K. L. Swanson (2012). On the origins of decadal climate variability: a network perspective. Nonlinear Processes in Geophysics **19**(5): 559-568.
- Valavanis, V. D., G. J. Pierce, A. F. Zuur, A. Palialexis, A. Saveliev, I. Katara and J. J. Wang (2008). Modelling of essential fish habitat based on remote sensing, spatial analysis and GIS. Hydrobiologia **612**: 5-20.

- Wang, B. (1995). Interdecadal changes in El Nino onset in the last 4 decades. Journal of Climate 8(2): 267-285.
- Wang, C. and P. C. Fiedler (2006). ENSO variability and the eastern tropical Pacific: A review. Progress in Oceanography 69(2-4): 239-266.
- Weickmann, K. M. (1991). El-Nino Southern Oscillation and Madden-Julian (30-60 day) oscillations during 1981-1982. Journal of Geophysical Research-Oceans 96: 3187-3195.
- Wyrki, K. and B. Kilonsky (1984). Mean water and current structure during The Hawaii -to -Tahiti shuttle experiment. Journal of Physical Oceanography 14: 242-254.
- Yasunaka, S. and K. Hanawa (2005). Regime shift in the global sea-surface temperatures: Its relation to El Nino-southern oscillation events and dominant variation modes. International Journal of Climatology 25(7): 913-930.
- Zainuddin, M., S.-i. Saitoh and K. Saitoh (2004). Detection of potential fishing ground for albacore tuna using synoptic measurements of ocean color and thermal remote sensing in the northwestern North Pacific. Geophysical Research Letters 31: L20311, 4 p.